

Improved Search for a Higgs Boson Produced in Association with $Z \rightarrow \ell^+ \ell^-$ in $p\bar{p}$ Collisions at $\sqrt{s} = 1.96$ TeV

T. Aaltonen,²² B. Álvarez González^{v,10} S. Amerio,⁴² D. Amidei,³³ A. Anastassov,³⁷ A. Annovi,¹⁸ J. Antos,¹³ G. Apollinari,¹⁶ J.A. Appel,¹⁶ A. Apresyan,⁴⁷ T. Arisawa,⁵⁶ A. Artikov,¹⁴ J. Asaadi,⁵² W. Ashmanskas,¹⁶ B. Auerbach,⁵⁹ A. Aurisano,⁵² F. Azfar,⁴¹ W. Badgett,¹⁶ A. Barbaro-Galtieri,²⁷ V.E. Barnes,⁴⁷ B.A. Barnett,²⁴ P. Barria^{ee,45} P. Bartos,¹³ M. Bauce^{cc,42} G. Bauer,³¹ F. Bedeschi,⁴⁵ D. Beecher,²⁹ S. Behari,²⁴ G. Bellettini^{dd,45} J. Bellinger,⁵⁸ D. Benjamin,¹⁵ A. Beretvas,¹⁶ A. Bhatti,⁴⁹ M. Binkley^{*},¹⁶ D. Bisello^{cc,42} I. Bizjak^{ii,29} K.R. Bland,⁵ C. Blocker,⁷ B. Blumenfeld,²⁴ A. Bocci,¹⁵ A. Bodek,⁴⁸ D. Bortoletto,⁴⁷ J. Boudreau,⁴⁶ A. Boveia,¹² B. Brau^{a,16} L. Brigliadori^{bb,6} A. Brisuda,¹³ C. Bromberg,³⁴ E. Brucken,²² M. Bucciantonio^{dd,45} J. Budagov,¹⁴ H.S. Budd,⁴⁸ S. Budd,²³ K. Burkett,¹⁶ G. Busetto^{cc,42} P. Bussey,²⁰ A. Buzatu,³² S. Cabrera^{x,15} C. Calancha,³⁰ S. Camarda,⁴ M. Campanelli,³⁴ M. Campbell,³³ F. Canelli^{12,16} A. Canepa,⁴⁴ B. Carls,²³ D. Carlsmith,⁵⁸ R. Carosi,⁴⁵ S. Carrillo^{k,17} S. Carron,¹⁶ B. Casal,¹⁰ M. Casarsa,¹⁶ A. Castro^{bb,6} P. Catastini,¹⁶ D. Cauz,⁵³ V. Cavaliere^{ee,45} M. Cavalli-Sforza,⁴ A. Cerri^{f,27} L. Cerrito^{q,29} Y.C. Chen,¹ M. Chertok,⁸ G. Chiarelli,⁴⁵ G. Chlachidze,¹⁶ F. Chlebana,¹⁶ K. Cho,²⁶ D. Chokheli,¹⁴ J.P. Chou,²¹ W.H. Chung,⁵⁸ Y.S. Chung,⁴⁸ C.I. Ciobanu,⁴³ M.A. Ciocci^{ee,45} A. Clark,¹⁹ D. Clark,⁷ G. Compostella^{cc,42} M.E. Convery,¹⁶ J. Conway,⁸ M. Corbo,⁴³ M. Cordelli,¹⁸ C.A. Cox,⁸ D.J. Cox,⁸ F. Crescioli^{dd,45} C. Cuenca Almenar,⁵⁹ J. Cuevas^{v,10} R. Culbertson,¹⁶ D. Dagenhart,¹⁶ N. d'Ascenzo^{t,43} M. Datta,¹⁶ P. de Barbaro,⁴⁸ S. De Cecco,⁵⁰ G. De Lorenzo,⁴ M. Dell'Orso^{dd,45} C. Deluca,⁴ L. Demortier,⁴⁹ J. Deng^{c,15} M. Deninno,⁶ F. Devoto,²² M. d'Errico^{cc,42} A. Di Canto^{dd,45} B. Di Ruzza,⁴⁵ J.R. Dittmann,⁵ M. D'Onofrio,²⁸ S. Donati^{dd,45} P. Dong,¹⁶ T. Dorigo,⁴² K. Ebina,⁵⁶ A. Elagin,⁵² A. Eppig,³³ R. Erbacher,⁸ D. Errede,²³ S. Errede,²³ N. Ershaidat^{aa,43} R. Eusebi,⁵² H.C. Fang,²⁷ S. Farrington,⁴¹ M. Feindt,²⁵ J.P. Fernandez,³⁰ C. Ferrazza^{ff,45} R. Field,¹⁷ G. Flanagan^{r,47} R. Forrest,⁸ M.J. Frank,⁵ M. Franklin,²¹ J.C. Freeman,¹⁶ I. Furic,¹⁷ M. Gallinaro,⁴⁹ J. Galyardt,¹¹ J.E. Garcia,¹⁹ A.F. Garfinkel,⁴⁷ P. Garosi^{ee,45} H. Gerberich,²³ E. Gerchtein,¹⁶ S. Giagu^{gg,50} V. Giakoumopoulou,³ P. Giannetti,⁴⁵ K. Gibson,⁴⁶ C.M. Ginsburg,¹⁶ N. Giokaris,³ P. Giromini,¹⁸ M. Giunta,⁴⁵ G. Giurgiu,²⁴ V. Glagolev,¹⁴ D. Glenzinski,¹⁶ M. Gold,³⁶ D. Goldin,⁵² N. Goldschmidt,¹⁷ A. Golossanov,¹⁶ G. Gomez,¹⁰ G. Gomez-Ceballos,³¹ M. Goncharov,³¹ O. González,³⁰ I. Gorelov,³⁶ A.T. Goshaw,¹⁵ K. Goulianos,⁴⁹ A. Gresele,⁴² S. Grinstein,⁴ C. Grosso-Pilcher,¹² R.C. Group,¹⁶ J. Guimaraes da Costa,²¹ Z. Gunay-Unalan,³⁴ C. Haber,²⁷ S.R. Hahn,¹⁶ E. Halkiadakis,⁵¹ A. Hamaguchi,⁴⁰ J.Y. Han,⁴⁸ F. Happacher,¹⁸ K. Hara,⁵⁴ D. Hare,⁵¹ M. Hare,⁵⁵ R.F. Harr,⁵⁷ K. Hatakeyama,⁵ C. Hays,⁴¹ M. Heck,²⁵ J. Heinrich,⁴⁴ M. Herndon,⁵⁸ S. Hewamanage,⁵ D. Hidas,⁵¹ A. Hocker,¹⁶ W. Hopkins^{g,16} D. Horn,²⁵ S. Hou,¹ R.E. Hughes,³⁸ M. Hurwitz,¹² U. Husemann,⁵⁹ N. Hussain,³² M. Hussein,³⁴ J. Huston,³⁴ G. Introzzi,⁴⁵ M. Iorigg^{o,50} A. Ivanov^{o,8} E. James,¹⁶ D. Jang,¹¹ B. Jayatilaka,¹⁵ E.J. Jeon,²⁶ M.K. Jha,⁶ S. Jindariani,¹⁶ W. Johnson,⁸ M. Jones,⁴⁷ K.K. Joo,²⁶ S.Y. Jun,¹¹ T.R. Junk,¹⁶ T. Kamon,⁵² P.E. Karchin,⁵⁷ Y. Kato^{n,40} W. Ketchum,¹² J. Keung,⁴⁴ V. Khotilovich,⁵² B. Kilminster,¹⁶ D.H. Kim,²⁶ H.S. Kim,²⁶ H.W. Kim,²⁶ J.E. Kim,²⁶ M.J. Kim,¹⁸ S.B. Kim,²⁶ S.H. Kim,⁵⁴ Y.K. Kim,¹² N. Kimura,⁵⁶ S. Klimenko,¹⁷ K. Kondo,⁵⁶ D.J. Kong,²⁶ J. Konigsberg,¹⁷ A. Korytov,¹⁷ A.V. Kotwal,¹⁵ M. Kreps,²⁵ J. Kroll,⁴⁴ D. Krop,¹² N. Krumnack^{l,5} M. Kruse,¹⁵ V. Krutelyov^{d,52} T. Kuhr,²⁵ M. Kurata,⁵⁴ S. Kwang,¹² A.T. Laasanen,⁴⁷ S. Lami,⁴⁵ S. Lammel,¹⁶ M. Lancaster,²⁹ R.L. Lander,⁸ K. Lannon^{u,38} A. Lath,⁵¹ G. Latino^{ee,45} I. Lazzizzera,⁴² T. LeCompte,² E. Lee,⁵² H.S. Lee,¹² J.S. Lee,²⁶ S.W. Lee^{w,52} S. Leo^{dd,45} S. Leone,⁴⁵ J.D. Lewis,¹⁶ C.-J. Lin,²⁷ J. Linacre,⁴¹ M. Lindgren,¹⁶ E. Lipeles,⁴⁴ A. Lister,¹⁹ D.O. Litvintsev,¹⁶ C. Liu,⁴⁶ Q. Liu,⁴⁷ T. Liu,¹⁶ S. Lockwitz,⁵⁹ N.S. Lockyer,⁴⁴ A. Loginov,⁵⁹ D. Lucchesi^{cc,42} J. Lueck,²⁵ P. Lujan,²⁷ P. Lukens,¹⁶ G. Lungu,⁴⁹ J. Lys,²⁷ R. Lysak,¹³ R. Madrak,¹⁶ K. Maeshima,¹⁶ K. Makhoul,³¹ P. Maksimovic,²⁴ S. Malik,⁴⁹ G. Manca^{b,28} A. Manousakis-Katsikakis,³ F. Margaroli,⁴⁷ C. Marino,²⁵ M. Martínez,⁴ R. Martínez-Ballarín,³⁰ P. Mastrandrea,⁵⁰ M. Mathis,²⁴ M.E. Mattson,⁵⁷ P. Mazzanti,⁶ K.S. McFarland,⁴⁸ P. McIntyre,⁵² R. McNulty^{i,28} A. Mehta,²⁸ P. Mehtala,²² A. Menzione,⁴⁵ C. Mesropian,⁴⁹ T. Miao,¹⁶ D. Mietlicki,³³ A. Mitra,¹ H. Miyake,⁵⁴ S. Moed,²¹ N. Moggi,⁶ M.N. Mondragon^{k,16} C.S. Moon,²⁶ R. Moore,¹⁶ M.J. Morello,¹⁶ J. Morlock,²⁵ P. Movilla Fernandez,¹⁶ A. Mukherjee,¹⁶ Th. Muller,²⁵ P. Murat,¹⁶ M. Mussini^{bb,6} J. Nachtman^{m,16} Y. Nagai,⁵⁴ J. Naganoma,⁵⁶ I. Nakano,³⁹ A. Napier,⁵⁵ J. Nett,⁵⁸ C. Neu^{z,44} M.S. Neubauer,²³ J. Nielsen^{e,27} L. Nodulman,² O. Norriella,²³ E. Nurse,²⁹ L. Oakes,⁴¹ S.H. Oh,¹⁵ Y.D. Oh,²⁶ I. Oksuzian,¹⁷ T. Okusawa,⁴⁰ R. Orava,²² L. Ortolan,⁴ S. Pagan Griso^{cc,42} C. Pagliarone,⁵³ E. Palencia^{f,10} V. Papadimitriou,¹⁶ A.A. Paramonov,² J. Patrick,¹⁶ G. Pauletta^{hh,53} M. Paulini,¹¹ C. Paus,³¹ D.E. Pellett,⁸

A. Penzo,⁵³ T.J. Phillips,¹⁵ G. Piacentino,⁴⁵ E. Pianori,⁴⁴ J. Pilot,³⁸ K. Pitts,²³ C. Plager,⁹ L. Pondrom,⁵⁸ K. Potamianos,⁴⁷ O. Poukhov*,¹⁴ F. Prokoshin^y,¹⁴ A. Pronko,¹⁶ F. Ptohos^h,¹⁸ E. Pueschel,¹¹ G. Punzi^{dd},⁴⁵ J. Pursley,⁵⁸ A. Rahaman,⁴⁶ V. Ramakrishnan,⁵⁸ N. Ranjan,⁴⁷ I. Redondo,³⁰ P. Renton,⁴¹ M. Rescigno,⁵⁰ F. Rimondi^{bb},⁶ L. Ristori^{45,16} A. Robson,²⁰ T. Rodrigo,¹⁰ T. Rodriguez,⁴⁴ E. Rogers,²³ S. Rolli,⁵⁵ R. Roser,¹⁶ M. Rossi,⁵³ F. Ruffini^{ee},⁴⁵ A. Ruiz,¹⁰ J. Russ,¹¹ V. Rusu,¹⁶ A. Safonov,⁵² W.K. Sakumoto,⁴⁸ L. Santi^{hh},⁵³ L. Sartori,⁴⁵ K. Sato,⁵⁴ V. Saveliev^t,⁴³ A. Savoy-Navarro,⁴³ P. Schlabach,¹⁶ A. Schmidt,²⁵ E.E. Schmidt,¹⁶ M.P. Schmidt*,⁵⁹ M. Schmitt,³⁷ T. Schwarz,⁸ L. Scodellaro,¹⁰ A. Scribano^{ee},⁴⁵ F. Scuri,⁴⁵ A. Sedov,⁴⁷ S. Seidel,³⁶ Y. Seiya,⁴⁰ A. Semenov,¹⁴ F. Sforza^{dd},⁴⁵ A. Sfyrta,²³ S.Z. Shalhout,⁸ T. Shears,²⁸ R. Shekhar,¹⁵ P.F. Shepard,⁴⁶ M. Shimojima^s,⁵⁴ S. Shiraishi,¹² M. Shochet,¹² I. Shreyber,³⁵ A. Simonenko,¹⁴ P. Sinervo,³² A. Sissakian*,¹⁴ K. Sliwa,⁵⁵ J.R. Smith,⁸ F.D. Snider,¹⁶ A. Soha,¹⁶ S. Somalwar,⁵¹ V. Sorin,⁴ P. Squillacioti,¹⁶ M. Stanitzki,⁵⁹ R. St. Denis,²⁰ B. Stelzer,³² O. Stelzer-Chilton,³² D. Stentz,³⁷ J. Strologas,³⁶ G.L. Strycker,³³ Y. Sudo,⁵⁴ A. Sukhanov,¹⁷ I. Suslov,¹⁴ K. Takemasa,⁵⁴ Y. Takeuchi,⁵⁴ J. Tang,¹² M. Tecchio,³³ P.K. Teng,¹ J. Thom^g,¹⁶ J. Thome,¹¹ G.A. Thompson,²³ E. Thomson,⁴⁴ P. Ttito-Guzmán,³⁰ S. Tkaczyk,¹⁶ D. Toback,⁵² S. Tokar,¹³ K. Tollefson,³⁴ T. Tomura,⁵⁴ D. Tonelli,¹⁶ S. Torre,¹⁸ D. Torretta,¹⁶ P. Totaro^{hh},⁵³ M. Trovato^{ff},⁴⁵ Y. Tu,⁴⁴ N. Turini^{ee},⁴⁵ F. Ukegawa,⁵⁴ S. Uozumi,²⁶ A. Varganov,³³ E. Vataga^{ff},⁴⁵ F. Vázquez^k,¹⁷ G. Velev,¹⁶ C. Vellidis,³ M. Vidal,³⁰ I. Vila,¹⁰ R. Vilar,¹⁰ M. Vogel,³⁶ G. Volpi^{dd},⁴⁵ P. Wagner,⁴⁴ R.L. Wagner,¹⁶ T. Wakisaka,⁴⁰ R. Wallny,⁹ S.M. Wang,¹ A. Warburton,³² D. Waters,²⁹ M. Weinberger,⁵² W.C. Wester III,¹⁶ B. Whitehouse,⁵⁵ D. Whiteson^c,⁴⁴ A.B. Wicklund,² E. Wicklund,¹⁶ S. Wilbur,¹² F. Wick,²⁵ H.H. Williams,⁴⁴ J.S. Wilson,³⁸ P. Wilson,¹⁶ B.L. Winer,³⁸ P. Wittich^g,¹⁶ S. Wolbers,¹⁶ H. Wolfe,³⁸ T. Wright,³³ X. Wu,¹⁹ Z. Wu,⁵ K. Yamamoto,⁴⁰ J. Yamaoka,¹⁵ T. Yang,¹⁶ U.K. Yang^p,¹² Y.C. Yang,²⁶ W.-M. Yao,²⁷ G.P. Yeh,¹⁶ K. Yi^m,¹⁶ J. Yoh,¹⁶ K. Yorita,⁵⁶ T. Yoshida^j,⁴⁰ G.B. Yu,¹⁵ I. Yu,²⁶ S.S. Yu,¹⁶ J.C. Yun,¹⁶ A. Zanetti,⁵³ Y. Zeng,¹⁵ and S. Zucchelli^{bb6}

(CDF Collaboration[†])

¹*Institute of Physics, Academia Sinica, Taipei, Taiwan 11529, Republic of China*

²*Argonne National Laboratory, Argonne, Illinois 60439, USA*

³*University of Athens, 157 71 Athens, Greece*

⁴*Institut de Fisica d'Altes Energies, Universitat Autònoma de Barcelona, E-08193, Bellaterra (Barcelona), Spain*

⁵*Baylor University, Waco, Texas 76798, USA*

⁶*Istituto Nazionale di Fisica Nucleare Bologna, ^{bb}University of Bologna, I-40127 Bologna, Italy*

⁷*Brandeis University, Waltham, Massachusetts 02254, USA*

⁸*University of California, Davis, Davis, California 95616, USA*

⁹*University of California, Los Angeles, Los Angeles, California 90024, USA*

¹⁰*Instituto de Fisica de Cantabria, CSIC-University of Cantabria, 39005 Santander, Spain*

¹¹*Carnegie Mellon University, Pittsburgh, Pennsylvania 15213, USA*

¹²*Enrico Fermi Institute, University of Chicago, Chicago, Illinois 60637, USA*

¹³*Comenius University, 842 48 Bratislava, Slovakia; Institute of Experimental Physics, 040 01 Kosice, Slovakia*

¹⁴*Joint Institute for Nuclear Research, RU-141980 Dubna, Russia*

¹⁵*Duke University, Durham, North Carolina 27708, USA*

¹⁶*Fermi National Accelerator Laboratory, Batavia, Illinois 60510, USA*

¹⁷*University of Florida, Gainesville, Florida 32611, USA*

¹⁸*Laboratori Nazionali di Frascati, Istituto Nazionale di Fisica Nucleare, I-00044 Frascati, Italy*

¹⁹*University of Geneva, CH-1211 Geneva 4, Switzerland*

²⁰*Glasgow University, Glasgow G12 8QQ, United Kingdom*

²¹*Harvard University, Cambridge, Massachusetts 02138, USA*

²²*Division of High Energy Physics, Department of Physics, University of Helsinki and Helsinki Institute of Physics, FIN-00014, Helsinki, Finland*

²³*University of Illinois, Urbana, Illinois 61801, USA*

²⁴*The Johns Hopkins University, Baltimore, Maryland 21218, USA*

²⁵*Institut für Experimentelle Kernphysik, Karlsruhe Institute of Technology, D-76131 Karlsruhe, Germany*

²⁶*Center for High Energy Physics: Kyungpook National University,*

Daegu 702-701, Korea; Seoul National University, Seoul 151-742,

Korea; Sungkyunkwan University, Suwon 440-746,

Korea; Korea Institute of Science and Technology Information,

Daejeon 305-806, Korea; Chonnam National University, Gwangju 500-757,

Korea; Chonbuk National University, Jeonju 561-756, Korea

²⁷*Ernest Orlando Lawrence Berkeley National Laboratory, Berkeley, California 94720, USA*

²⁸*University of Liverpool, Liverpool L69 7ZE, United Kingdom*

²⁹*University College London, London WC1E 6BT, United Kingdom*

³⁰*Centro de Investigaciones Energeticas Medioambientales y Tecnológicas, E-28040 Madrid, Spain*

- ³¹Massachusetts Institute of Technology, Cambridge, Massachusetts 02139, USA
³²Institute of Particle Physics: McGill University, Montréal, Québec, Canada H3A 2T8; Simon Fraser University, Burnaby, British Columbia, Canada V5A 1S6; University of Toronto, Toronto, Ontario, Canada M5S 1A7; and TRIUMF, Vancouver, British Columbia, Canada V6T 2A3
³³University of Michigan, Ann Arbor, Michigan 48109, USA
³⁴Michigan State University, East Lansing, Michigan 48824, USA
³⁵Institution for Theoretical and Experimental Physics, ITEP, Moscow 117259, Russia
³⁶University of New Mexico, Albuquerque, New Mexico 87131, USA
³⁷Northwestern University, Evanston, Illinois 60208, USA
³⁸The Ohio State University, Columbus, Ohio 43210, USA
³⁹Okayama University, Okayama 700-8530, Japan
⁴⁰Osaka City University, Osaka 588, Japan
⁴¹University of Oxford, Oxford OX1 3RH, United Kingdom
⁴²Istituto Nazionale di Fisica Nucleare, Sezione di Padova-Trento, ^{cc}University of Padova, I-35131 Padova, Italy
⁴³LPNHE, Université Pierre et Marie Curie/IN2P3-CNRS, UMR7585, Paris, F-75252 France
⁴⁴University of Pennsylvania, Philadelphia, Pennsylvania 19104, USA
⁴⁵Istituto Nazionale di Fisica Nucleare Pisa, ^{dd}University of Pisa, ^{ee}University of Siena and ^{ff}Scuola Normale Superiore, I-56127 Pisa, Italy
⁴⁶University of Pittsburgh, Pittsburgh, Pennsylvania 15260, USA
⁴⁷Purdue University, West Lafayette, Indiana 47907, USA
⁴⁸University of Rochester, Rochester, New York 14627, USA
⁴⁹The Rockefeller University, New York, New York 10065, USA
⁵⁰Istituto Nazionale di Fisica Nucleare, Sezione di Roma 1, ^{gg}Sapienza Università di Roma, I-00185 Roma, Italy
⁵¹Rutgers University, Piscataway, New Jersey 08855, USA
⁵²Texas A&M University, College Station, Texas 77843, USA
⁵³Istituto Nazionale di Fisica Nucleare Trieste/Udine, I-34100 Trieste, ^{hh}University of Trieste/Udine, I-33100 Udine, Italy
⁵⁴University of Tsukuba, Tsukuba, Ibaraki 305, Japan
⁵⁵Tufts University, Medford, Massachusetts 02155, USA
⁵⁶Waseda University, Tokyo 169, Japan
⁵⁷Wayne State University, Detroit, Michigan 48201, USA
⁵⁸University of Wisconsin, Madison, Wisconsin 53706, USA
⁵⁹Yale University, New Haven, Connecticut 06520, USA

We present a search for the standard model Higgs boson produced with a Z boson in 4.1 fb^{-1} of data collected with the CDF II detector at the Tevatron. In events consistent with the decay of the Higgs boson to a bottom-quark pair and the Z boson to electrons or muons, we set 95% credibility level upper limits on the ZH production cross section times the $H \rightarrow b\bar{b}$ branching ratio. Improved analysis methods enhance signal sensitivity by 20% relative to previous searches beyond the gain due to the larger data sample. At a Higgs boson mass of $115 \text{ GeV}/c^2$ we set a limit of 5.9 times the standard model value.

PACS numbers: 14.80.Bn, 13.85.Rm

*Deceased

†With visitors from ^aUniversity of Massachusetts Amherst, Amherst, Massachusetts 01003, ^bIstituto Nazionale di Fisica Nucleare, Sezione di Cagliari, 09042 Monserrato (Cagliari), Italy, ^cUniversity of California Irvine, Irvine, CA 92697, ^dUniversity of California Santa Barbara, Santa Barbara, CA 93106 ^eUniversity of California Santa Cruz, Santa Cruz, CA 95064, ^fCERN, CH-1211 Geneva, Switzerland, ^gCornell University, Ithaca, NY 14853, ^hUniversity of Cyprus, Nicosia CY-1678, Cyprus, ⁱUniversity College Dublin, Dublin 4, Ireland, ^jUniversity of Fukui, Fukui City, Fukui Prefecture, Japan 910-0017, ^kUniversidad Iberoamericana, Mexico D.F., Mexico, ^lIowa State University, Ames, IA 50011, ^mUniversity of Iowa, Iowa City, IA 52242, ⁿKinki University, Higashi-Osaka City, Japan 577-8502, ^oKansas State University, Manhattan, KS 66506, ^pUniversity of Manchester, Manchester M13

Establishing the mechanism of electroweak symmetry breaking (EWSB) is one of the outstanding issues of particle physics. In the standard model (SM), EWSB is

9PL, England, ^qQueen Mary, University of London, London, E1 4NS, England, ^rMuons, Inc., Batavia, IL 60510, ^sNagasaki Institute of Applied Science, Nagasaki, Japan, ^tNational Research Nuclear University, Moscow, Russia, ^uUniversity of Notre Dame, Notre Dame, IN 46556, ^vUniversidad de Oviedo, E-33007 Oviedo, Spain, ^wTexas Tech University, Lubbock, TX 79609, ^xIFIC(CSIC-Universitat de Valencia), 56071 Valencia, Spain, ^yUniversidad Tecnica Federico Santa Maria, 110v Valparaiso, Chile, ^zUniversity of Virginia, Charlottesville, VA 22906, ^{aa}Yarmouk University, Irbid 211-63, Jordan, ⁱⁱOn leave from J. Stefan Institute, Ljubljana, Slovenia,

mediated by a Higgs field that manifests a particle, the as-yet-unobserved Higgs boson. A SM Higgs boson with mass (M_H) below $114.4 \text{ GeV}/c^2$ or with M_H between 162 and $166 \text{ GeV}/c^2$ has been excluded at 95% confidence level in direct searches at LEP [1] and the Tevatron [2]. A recently reported [3] preliminary update of the Tevatron result has expanded this 95% exclusion range to values of M_H between 158 and $175 \text{ GeV}/c^2$.

At the Tevatron, production of the Higgs boson is dominated by the direct production process $gg \rightarrow H$, and for $M_H < 135 \text{ GeV}/c^2$ the Higgs boson decays primarily to a pair of b quarks, $H \rightarrow b\bar{b}$ [4]. The process $gg \rightarrow H \rightarrow b\bar{b}$ is overwhelmed by multi-jet background. Associated production of a Higgs boson with a leptonically decaying W or Z boson yields a distinct signature for efficient selection and in turn greater sensitivity despite a significantly smaller cross section than direct production [5, 6]. This Letter presents an improved search for the SM Higgs boson produced in association with a Z boson, $ZH \rightarrow \ell^+\ell^-b\bar{b}$ (where ℓ is either an electron, e , or muon, μ) using $1.96 \text{ TeV } p\bar{p}$ collision data corresponding to 4.1 fb^{-1} of integrated luminosity collected with the CDF II detector [7]. This search channel is one of the most sensitive to a low-mass SM Higgs boson at the Tevatron [8, 9].

Previous CDF efforts in this mode used an artificial neural network classifier (NN) [10] or a likelihood based on matrix-element probabilities (MEP) [11] for signal isolation. Here we enhance these techniques with NN-based b jet discrimination [12, 13] and an improved multivariate jet-energy correction to improve background rejection. New $Z \rightarrow e^+e^-$ selections increase the acceptance of ZH signal, and new combinations of b jet identifiers yield better signal sensitivity, as reflected in the expected cross section limit. These additions improve the expected sensitivity by a factor of 1.2 over the gain expected just from additional integrated luminosity.

The selection requirements most relevant to this analysis are discussed below; a detailed presentation can be found in [14]. We select ZH candidates by first identifying a sample of events containing a $Z \rightarrow \ell^+\ell^-$ decay. Events are selected in real time (triggered) based on the presence of high- p_T electron and muon [15] candidates. The majority ($\sim 80\%$) of ZH candidates pass the trigger selection requiring events to contain at least one central ($|\eta| \leq 1.0$) track of $p_T \geq 9 \text{ GeV}/c$ matched to an electromagnetic energy (EM) cluster of $E_T \geq 18 \text{ GeV}$ (a trigger electron) or at least one central track of $p_T \geq 20 \text{ GeV}/c$ pointing to signals in the muon detectors (a trigger muon). The remaining fraction of ZH candidate events comes from newly included data selected by a trigger that requires two or more EM clusters of $E_T \geq 18 \text{ GeV}$ and $|\eta| \leq 3.6$ without requiring that the clusters are associated with tracks (trackless trigger). Events are further required to contain a lepton pair that forms a Z candidate with mass in the range $76 \leq M_{\ell\ell} \leq 106 \text{ GeV}/c^2$. Pairs of

central leptons forming Z candidates must have opposite charge; electrons in the forward ($|\eta| > 1.0$) acceptance of the detector may not have an associated track and no charge requirement is imposed.

We divide the Z candidates into two categories based on signal-to-background ratio (S/B). The search for the signal in these two categories is conducted separately to improve sensitivity to a ZH signal. The high- S/B category includes Z candidates formed from a trigger muon and a second muon candidate with $p_T \geq 10 \text{ GeV}/c$, or a trigger electron paired with a second electron candidate formed from either a central EM cluster of $E_T \geq 10 \text{ GeV}$ matched to a track of $p_T \geq 5 \text{ GeV}/c$ or a forward EM cluster of $E_T \geq 18 \text{ GeV}$. The low- S/B category contains Z candidates in events satisfying the trackless trigger only or formed from a trigger electron paired with an isolated central track with $p_T \geq 20 \text{ GeV}/c$ pointing to an uninstrumented region of the calorimeter. The low- S/B category is included for the first time in the search for ZH production at CDF.

Higgs boson candidates are assembled from pairs of jets. We form jets from energy deposits in the calorimeter using the JETCLU algorithm [16] with a cone radius of 0.4. We consider only jets well contained in the calorimeter, $|\eta| \leq 2.0$, and well separated from the Z -decay leptons, $\Delta R \geq 0.4$ [17]. Measured jet energies are corrected to account for η -dependent variations in detector response, calorimeter coverage, and the expected contribution from additional $p\bar{p}$ pair interactions in the same event [18]. Events are required to have one jet with $E_T \geq 25 \text{ GeV}$ and a second of $E_T \geq 15 \text{ GeV}$. We refer to the events containing a Z boson candidate and two such jets as the PreTag sample; b quark identification (described below) is applied to the PreTag sample to form our final analysis samples. There are 11,806 (3,061) events in the high (low) S/B PreTag data sample, wherein we expect 5.0 ± 0.7 (0.8 ± 0.1) ZH signal events for $M_H = 115 \text{ GeV}/c^2$. Inclusion of the low- S/B subsample increases the total signal yield in the PreTag sample by 16%.

The PreTag sample consists mainly of Z +light flavor (l.f.) jet (u, d, s, g) events, with smaller contributions from Z +heavy flavor (h.f.) jet (c, b), $t\bar{t}$, and diboson processes. To reduce the Z +l.f. background, we look for b jets in the event. We use two algorithms to identify (tag) b jets: one based on evidence for a decay displaced spatially from the $p\bar{p}$ interaction point (SV) [7] and one based on track impact parameters with respect to the $p\bar{p}$ interaction point (JP) [19]. For the SV algorithm, there are two operating points: tight and loose [20]. The tight operating point has better l.f.-jet rejection (smaller mistag probability) at the expense of reduced b -jet identification efficiency.

We select events in the PreTag sample using the b tagging algorithms on the jet pairs forming Higgs candidates. We require the jet pairs to satisfy one of the following classifications, in order of precedence from highest to lowest ratio of ZH signal to background: a pair

containing two SV-tight-tagged jets is classified as tight-double-tagged (TDT); a pair consisting of one SV-loose-tagged jet and a second JP-tagged jet is classified as loose-double-tagged (LDT); and a pair where only one jet has a SV-tight-tag is classified as single-tagged (ST). When there are multiple $H \rightarrow b\bar{b}$ candidates in an event, the jet pair with the highest b tag class is selected (TDT > LDT > ST). This is the first time the JP algorithm has been used in the $ZH \rightarrow \ell^+\ell^-b\bar{b}$ channel. While the b tag selection matches the signal selection efficiency (approximately 60%) and background rejection rate (96%) of previous efforts, the addition of the new LDT class increases sensitivity to a ZH signal by 6%. Due to differing background composition, the events are divided into independent subsamples based on b -tagging class. With two Z boson S/B categories and three b -tagging classes, we form a total of six subsamples that we analyze for ZH content.

We compare the b -tag data to a model of signal and backgrounds to estimate the signal content. Signal, $t\bar{t}$, and diboson events are modeled with the PYTHIA [21] event generator. Backgrounds from Z +h.f. processes are simulated at the quark level using ALPGEN [22], then passed to PYTHIA for hadronization. The detector response is modeled with a detailed detector simulation [7]. We estimate the background from Z +l.f. mistags using re-weighted PreTag data with weights reflecting the probability for a l.f. jet to be erroneously b tagged. A small fraction, much less than 1%, of jets can be erroneously identified as electrons, resulting in a background of misidentified (misID) $Z \rightarrow ee$ candidates. The likelihood of jet-electron misidentification is measured in generic jet data and applied to all electron-jet and jet-jet pairings in the electron triggered samples to generate a model of misID Z events. The misID $Z \rightarrow \mu\mu$ background contribution is estimated from the events passing all selection requirements but containing like-charge muon pairs. Predicted and observed event totals are listed in Table I for the b -tagged subsamples.

To improve the separation of ZH from background, we utilize several multivariate techniques that use kinematic quantities as inputs. The dijet mass M_{jj} is one of the most useful quantities, with its separating power limited mainly by the jet-energy resolution. In ZH signal events with $Z \rightarrow \ell^+\ell^-$, incorrect measurement of jet energies results in apparent missing transverse energy \cancel{E}_T [23]. We correct jet energies, based upon the \cancel{E}_T , and thereby improve the resolution on the dijet invariant mass. Jet-energy correction factors are computed by a NN trained to match measured jet energies to parton-level energies in Z +jets and signal events. In this analysis, this neural network is improved compared to the previous analysis [10] by utilizing additional input variables describing the recoil of the Z boson. The corrected jet energies are used to recompute the Higgs candidate mass M_H , the p_T of the jets, the p_T of the Higgs candi-

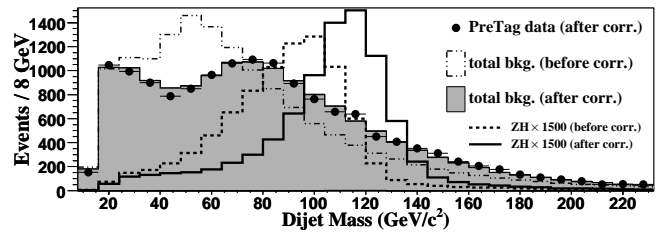


FIG. 1: The dijet invariant mass distribution of the two jets with the highest E_T in the PreTag sample. The distribution is shown for data after NN correction of jet energies. The dijet mass is shown for background before (dash-dotted line) and after (grey region) NN correction. The dotted (solid) curves show the dijet mass for signal ($M_H = 115 \text{ GeV}/c^2$ and scaled by a factor of 1500) before (after) correction.

date, the projection of $\vec{\cancel{E}}_T$ onto the lower- E_T Higgs jet, and the sphericity. The effect of the NN corrections on the reconstructed $H \rightarrow b\bar{b}$ mass is shown in Fig. 1. In signal the resolution [24] on M_H is improved from about 18% to 12%.

To exploit the combined signal-to-background discrimination power of event quantities and their correlations, we employ a neural network discriminant (NN_D) trained to simultaneously separate ZH , $t\bar{t}$, and Z +jets events. The NN_D is configured to return values of $(x, y) = (1, 0)$ for ZH events, $(0, 0)$ for Z +jets, and $(1, 1)$ for $t\bar{t}$. A separate NN_D is formed for each of the three b -tag classes. In addition to the quantities recomputed with corrected jet energies, the NN_D inputs include: \cancel{E}_T ; MEPs for ZH , $t\bar{t}$, and Z +jets processes; the number of jets in the event; and the output of a b jet identifying artificial neural network (NN_b) [12]. The ZH process MEP is computed [11] by convolving the theoretical matrix element for ZH production with detector resolution functions. The resulting MEP reflects the likelihood that an event is signal. We calculate two additional MEPs under the hypotheses that an event is Z +jets or $t\bar{t}$ to aid background rejection. The NN_b augments the performance of the SV algorithm by isolating incorrectly b -tagged l.f. jets. The addition of NN_b as an input enhances the ability of the NN_D to distinguish ZH from Z +l.f., which constitutes 40% of the total background in the ST class. One-dimensional projections of NN_D output are shown in Fig. 2 for each b -tag class.

The effect of systematic uncertainties on the determination of signal content requires propagating uncertainties on NN_D input quantities to the output distributions. The dominant effect on the result comes from uncertainties on cross sections for background processes — a 40% uncertainty is assumed on the normalization of Z +h.f. samples [25], 11.5% for the diboson samples [26], 20% to account for the theoretical and experimental uncertainty on the $t\bar{t}$ cross section [27], and 5% for ZH signal [28]. Uncertainties of 4% (ST), 8% (TDT), and 11%

TABLE I: Comparison of the expected mean event totals for background and ZH signal with the observed number of data events. The totals are for full event selection, and systematic and statistical uncertainties are combined in quadrature. Systematic uncertainties dominate. The background composition is provided in the first five rows. Each of the six ZH subsamples is presented in a separate column.

Process	High S/B			Low S/B		
	TDT	LDT	ST	TDT	LDT	ST
$t\bar{t}$	7.0 ± 1.5	8 ± 2	17 ± 4	2.9 ± 0.6	3.2 ± 0.8	8.9 ± 1.9
Diboson	2.9 ± 0.4	4 ± 1	16 ± 2	0.5 ± 0.1	0.6 ± 0.1	3.3 ± 0.5
$Z + \text{h.f.}$	18 ± 7	30 ± 13	159 ± 67	3.5 ± 1.5	5.6 ± 2.4	32 ± 14
$Z + \text{l.f.}$	0.9 ± 0.3	9 ± 3	152 ± 23	0.4 ± 0.1	3.8 ± 1.3	50 ± 7.6
misID Z	0.7 ± 0.3	2 ± 1	22 ± 11	1.4 ± 0.7	1.1 ± 0.5	23 ± 12
Total Bkg.	29 ± 8	53 ± 14	366 ± 72	9 ± 2	14 ± 3	117 ± 20
$ZH(115 \text{ GeV}/c^2)$	0.7 ± 0.1	0.7 ± 0.1	1.7 ± 0.2	0.11 ± 0.01	0.11 ± 0.03	0.28 ± 0.05
Data	23	56	406	12	14	116

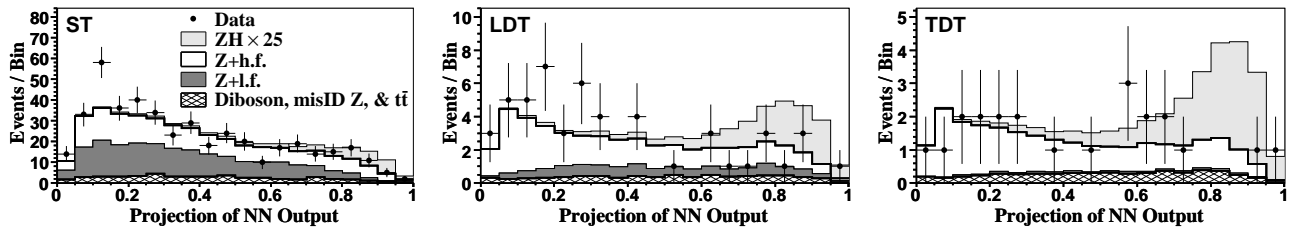


FIG. 2: Projections of the two-dimensional neural network (NN_D) output onto the x -axis (x and y are defined in the text) for events in the b -tag categories ST, LDT, and TDT. Events with a NN_D score of $y \geq 0.1$ are omitted to highlight the signal region. The ZH contribution is shown, multiplied by a factor of 25, for $M_H = 115 \text{ GeV}/c^2$.

(LDT) on the normalization of b -tagged samples are applied to account for different b -tag efficiencies in data and simulation. Other uncertainties affecting sample normalizations include: 6% on the integrated luminosity, 1% on the trigger and lepton reconstruction efficiencies [29], 1.5% on the measurement of lepton energies, and a 50% uncertainty on the total lepton misID estimate. We include uncertainties on jet energies, the modeling of initial and final state radiation, and mistag event weighting as variations on the shape and normalization of the NN_D output.

We calculate a limit on the associated production of a SM Higgs boson and Z boson based on the comparison of the full NN_D output of the b -tagged data to expectations for signal and background. We consider eleven Higgs mass hypotheses between 100 and $150 \text{ GeV}/c^2$. We use a Bayesian algorithm [30] with a flat prior in the production cross section, integrating over the priors for the systematic uncertainties, incorporating correlated rate and shape uncertainties, and uncorrelated bin-by-bin statistical uncertainties [31]. Systematic uncertainties reduce the sensitivity of this search by 16%. The expected 95% credibility level (C.L.) limits are calculated assuming no signal, based on expected backgrounds only, as the median of 1000 simulated experiments. The $\pm 1\sigma$ and $\pm 2\sigma$ expected limits are derived from the distribution of the

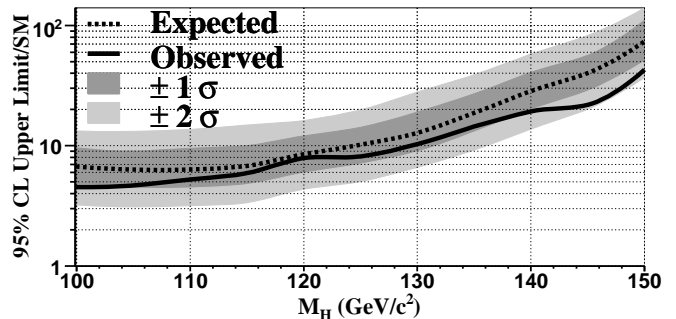


FIG. 3: The expected (dashed curve) and observed (solid curve) ZH cross section upper limits divided by the SM cross section are shown as a function of the Higgs boson mass. The dark (light) band represents the $\pm 1\sigma$ ($\pm 2\sigma$) expected limit range.

simulation limits at the 16th, 84th, 2nd, and 98th percentiles of the distribution, respectively. The observed 95% C.L. on the ZH cross section are calculated from the b -tagged data, and displayed in Fig. 3 and summarized in Table II.

In conclusion, we have searched for the SM Higgs boson produced in association with a Z boson, where $Z \rightarrow \ell^+ \ell^-$ and $H \rightarrow b\bar{b}$, finding no significant evidence for the process. We set 95% C.L. upper limits on the ZH produc-

TABLE II: Expected (Exp.) and observed (Obs.) 95% C.L. upper limits on the ZH production cross section times the branching ratio for $H \rightarrow b\bar{b}$ normalized to the SM value for Higgs masses between 100 and 150 GeV/ c^2 . The assumed ZH cross section and branching fraction for $H \rightarrow b\bar{b}$ are 0.11 pb [5, 6] and 0.73 [4] for a 115 GeV/ c^2 Higgs boson.

M_H	100	105	110	115	120	125	130	135	140	145	150
Exp.	6.7	6.4	6.3	6.8	8.5	10.	13	19	29	45	74
Obs.	4.5	4.6	5.3	5.9	7.9	8.1	10.	14	19	24	43

tion cross section times the $H \rightarrow b\bar{b}$ branching ratio for Higgs boson masses between 100 and 150 GeV/ c^2 . For a Higgs boson mass of 115 GeV/ c^2 we set (expect) a 95% C.L. upper limit of 5.9 (6.8) times the standard model prediction. This result is an important step forward in the search for the Higgs boson and the source of EWSB, improving upon the previous observed (expected) limits in this channel by factors of 2.2 to 3.7 (1.9 to 2.4).

We thank the Fermilab staff and the technical staffs of the participating institutions for their vital contributions. This work was supported by the U.S. Department of Energy and National Science Foundation; the Italian Istituto Nazionale di Fisica Nucleare; the Ministry of Education, Culture, Sports, Science and Technology of Japan; the Natural Sciences and Engineering Research Council of Canada; the National Science Council of the Republic of China; the Swiss National Science Foundation; the A.P. Sloan Foundation; the Bundesministerium für Bildung und Forschung, Germany; the World Class University Program, the National Research Foundation of Korea; the Science and Technology Facilities Council and the Royal Society, UK; the Institut National de Physique Nucleaire et Physique des Particules/CNRS; the Russian Foundation for Basic Research; the Ministerio de Ciencia e Innovación, and Programa Consolider-Ingenio 2010, Spain; the Slovak R&D Agency; and the Academy of Finland.

[1] R. Barate *et al.* (LEP Working Group), Phys. Lett. B **565**, 61 (2003).
[2] T. Aaltonen *et al.* (CDF and D0 Collaborations), Phys. Rev. Lett. **104**, 061802 (2010).
[3] The TEVNPH Working Group (CDF and D0 Collaborations) (2010), arXiv:1007.4587.
[4] A. Djouadi, J. Kalinowski, and M. Spira, Comput. Phys. Commun. **108**, 56 (1998).
[5] O. Brein, A. Djouadi, and R. Harlander, Phys. Lett. **B579**, 149 (2004), hep-ph/0307206.

[6] M. L. Ciccolini, S. Dittmaier, and M. Kramer, Phys. Rev. **D68**, 073003 (2003), hep-ph/0306234.
[7] D. Acosta *et al.* (CDF Collaboration), Phys. Rev. D **71**, 052003 (2005).
[8] T. Aaltonen *et al.* (CDF Collaboration), Phys. Rev. Lett. **103**, 101802 (2009).
[9] T. Aaltonen *et al.* (CDF Collaboration), Phys. Rev. Lett. **104**, 141801 (2010).
[10] T. Aaltonen *et al.* (CDF Collaboration), Phys. Rev. Lett. **101**, 251803 (2008).
[11] T. Aaltonen *et al.* (CDF Collaboration), Phys. Rev. D **80**, 071101 (2009).
[12] S. Richter (2007), Ph.D. Thesis, Karlsruhe U., EKP, FERMILAB-THESIS-2007-35.
[13] T. Aaltonen *et al.* (CDF) (2010), submitted to Phys. Rev. D, arXiv:1004.1181.
[14] S. Z. Shalhout (2010), Ph.D. Thesis, Wayne State Univ., FERMILAB-THESIS-2010-33.
[15] We use a cylindrical coordinate system with z along the proton beam direction, r the perpendicular radius from the central axis of the detector, and ϕ the azimuthal angle. For θ the polar angle from the proton beam, we define $\eta = -\ln \tan(\theta/2)$, transverse momentum $p_T = p \sin \theta$ and transverse energy $E_T = E \sin \theta$.
[16] G. Blazey and B. Flaughner, Ann. Rev. Nucl. Part. Sci. **49**, 633 (1999).
[17] The ΔR between two objects is given by $\sqrt{\Delta\eta^2 + \Delta\phi^2}$.
[18] A. Bhatti *et al.*, Nucl. Instrum. Methods Phys. Res., Sect. A **566**, 375 (2006).
[19] A. Abulencia *et al.* (CDF Collaboration), Phys. Rev. D **74**, 072006 (2006).
[20] C. Neu for the CDF Collaboration, presented at TOP 2006, Coimbra, Portugal, 12-15 Jan 2006.
[21] T. Sjöstrand *et al.*, Comput. Phys. Comm. **135**, 238 (2001). We use “PYTHIA Tune A”, R. Field and R. C. Group, hep-ph/0510198v1.
[22] M. L. Mangano *et al.*, J. High Energy Phys. **07**, 001 (2003).
[23] The missing E_T (\vec{E}_T) is defined by the sum over calorimeter towers: $\vec{E}_T = -\sum_i E_T^i \hat{n}_i$, where i = calorimeter tower number with $|\eta| < 3.6$, \hat{n}_i is a unit vector perpendicular to the beam axis and pointing at the i^{th} calorimeter tower. We also define $E_{\cancel{T}} = |\vec{E}_T|$.
[24] We define dijet mass resolution as the standard deviation of the dijet mass distribution divided by its mean.
[25] J. M. Campbell and R. K. Ellis, Phys. Rev. D **62**, 114012 (2000).
[26] J. M. Campbell and R. K. Ellis, Phys. Rev. D **60**, 113006 (1999).
[27] U. Langenfeld, S. Moch, and P. Uwer, Phys. Rev. D **80**, 054009 (2009).
[28] J. Baglio and A. Djouadi (2010), arXiv:1003.4266.
[29] D. Acosta *et al.*, Nucl. Instrum. Methods Phys. Res., Sect. A **494**, 57 (2002).
[30] K. Nakamura *et al.* (Particle Data Group), J. Phys. G **37**, 075021 (2010).
[31] T. Aaltonen *et al.* (CDF Collaboration), Phys. Rev. D **80**, 012002 (2009).